

# Modeling of a Controllable Drogue and Simulation of Hose-Drogue Refueling Systems Under Aerodynamic Disturbances

NIO Zi Feng, ZOU Guiyun, LIU Xueqiang\*

College of Aerospace Engineering, Nanjing University of Aeronautics and Astronautics, Nanjing 210016, P. R. China

(Received 9 June 2023; revised 12 October 2023; accepted 21 June 2024)

**Abstract:** A dynamic model of a stabilized drogue with four control surfaces is developed to mitigate the aerodynamic disturbances caused by the bow wave effect and wind turbulence during the docking stage of hose-drogue systems. Numerical simulations are used to identify the aerodynamic characteristics of the drogue, and the data is simplified using linear and polynomial functions. The aerodynamic model is used to design a linear quadratic regulator (LQR) controller. MATLAB/Simulink is used to construct a hose-drogue model and verify the effectiveness of the actively controllable stabilized drogue in reducing the effect of disturbances. The study also investigates the effects of control surface deflection angles on hose catenary curves using a static model. Numerical simulations show that the actively controllable stabilized drogue reduces the effects of the bow wave and wind turbulence, which maintains the stability of the hose-drogue system and improves the success rate of aerial refueling.

**Key words:** actively controllable drogue; hose-drogue aerial refueling; computational fluid dynamic (CFD); aerodynamic disturbance; linear quadratic regulator (LQR) controller

**CLC number:** V211.3

**Document code:** A

**Article ID:** 1005-1120(2024)03-0325-19

## 0 Introduction

In modern warfare, aerial refueling technology has emerged as a crucial element for achieving victory on the battlefield. As militaries continuously evolve their tactics, control over the seas and air has become a pivotal strategic requirement. Aerial refueling enables military forces to sustain their presence in the sky by aerial refueling thereby allowing extended operations to be conducted, gaining dominance over hostile airspace. With the rise of unmanned drone strikes, aerial sniping, and swarm drone tactics as seen in the Russo-Ukrainian War, and the strategic thinking evolution of the US military post-Gulf War, air and sea control is now imperative for conducting sustained bombing campaigns and surgical strikes on enemy targets, resources, and key personnel. Ultimately, achieving control over the skies and seas has become one of

the critical components of modern warfare, and aerial refueling has become an essential asset for conducting aerial operations.

There are currently two types of aerial refueling methods: The boom and receptacle (flying boom) and the probe and drogue. The probe and drogue method is more advantageous than the flying boom method due to its smaller size, simpler structure, and ability to simultaneously refuel multiple aircraft<sup>[1]</sup>. Consequently, the probe and drogue method is the most widely used among the two. Regardless of advantages of the probe and drogue system, the hose and drogue aerial refueling system is disrupted by various types of turbulences, including the wind gust and the bow wave or forebody effect. To achieve autonomous or automated refueling, control systems with artificial intelligence and machine learning have been developed. However, to further reduce disturbances, optimization of the

\*Corresponding author, E-mail address: liuxq@nuaa.edu.cn.

**How to cite this article:** NIO Zi Feng, ZOU Guiyun, LIU Xueqiang. Modeling of a controllable drogue and simulation of hose-drogue refueling systems under aerodynamic disturbances[J]. Transactions of Nanjing University of Aeronautics and Astronautics, 2024, 41(3):325-343.

<http://dx.doi.org/10.16356/j.1005-1120.2024.03.006>

aerodynamic characteristics of the refueling device (the refueling drogue) is also necessary.

Numerous studies have been conducted to examine the hose and drogue model and develop solutions to mitigate the negative impact of aerodynamic disturbances, such as turbulence and the bow wave effect. Additionally, research has investigated the influence of receiver aircraft on the hose-drogue system, as a clear understanding of the dynamic behaviors induced by an approaching receiver is essential for successful refueling missions. NASA<sup>[2]</sup> conducted aerial refueling flight tests using two F-18 aircraft to study the effects of bow waves and wake flows on the hose-drogue system. To understand the effect of bow waves and wake flows, the receiving aircraft performed vertical and horizontal sweep maneuvers that were observed during the aerial refueling process. The tests revealed that wind turbulence had a more significant effect on the drogue position than the presence of the receiving aircraft.

Ro et al.<sup>[3-4]</sup> conducted a study on formulating a model for a hose made up of interconnected rigid links, which could be affected by both gravitational and aerodynamic loads, including the wake of a tanker. They also designed an adjustable aerodynamic model to examine how manipulating the position of the drogue assembly drag could impact the location of the hose relative to the tanker, across various tanker movements and speeds. They also explored the dynamic behavior of the drogue assembly under different conditions, including atmospheric turbulence, pitch doublet maneuver of the tanker, and specific motions of the tanker such as climbing, descending, and phugoid oscillations. Furthermore, their study was expanded to examine the effect of the receiver bow wave effect on the drogue motion during the docking stage<sup>[5]</sup>. Moreover, they presented a new approach for stabilizing the drogue in the probe-drogue aerial refueling system<sup>[6]</sup>. The approach involves an active stabilization mechanism that employs four aerodynamic control surfaces to minimize alterations to the existing hose-drogue refueling system. The research thoroughly investigates the proposed method for active drogue stabili-

zation, presenting a design concept that demonstrates a significant decrease in drogue movement caused by gusts during wind tunnel testing.

Bhandari et al.<sup>[7]</sup> studied the bow wave effect in probe and drogue aerial refueling. They employed the Rankine aerodynamic model to approximate airflow around the receiver aircraft's nose. FELDMA-NN<sup>[8]</sup> developed a refueling drogue system and it improved the stability of the drogue by controlling the orientation of an annular duct that contains a small airfoil attached to the drogue's surface. The system employed an actuator and a ram air turbine that changed the orientation of the duct to enhance control over the drogue's movement in the presence of disturbances. This innovative system offered improved drogue stability and demonstrated the potential for engineering solutions that utilized advanced technologies in aerospace applications. Williamson et al.<sup>[9]</sup> presented a new method for stabilizing an automated refueling drogue in the presence of winds or receiver bow wave effects. The technique involved manipulating the drogue canopy to stabilize the drogue automatically. This approach ensured optimal control and stability during refueling operations, contributing to improved efficiency. The innovative design showcased the potential of modern engineering solutions and offered promising results for aerial refueling missions.

Numerous studies have demonstrated the significance of drogue stability control during aerial refueling operations. Successfully capturing the drogue is heavily dependent on the pilot's ability to predict its movement, and stabilizing the drogue under turbulence can be aided by a controllable drogue.

This study is an extension of experimental research conducted on the actively stabilized drogue by Ro et al.<sup>[6]</sup>. Their study predominantly centered on experimental approaches, leaving a gap in the comprehensive numerical analysis of drogue systems. This research expands upon their work by incorporating the receiver's bow wave effect and wind turbulence as the disturbances and utilizing numerical simulations for a comprehensive analysis.

This research expands the scope of analysis by

introducing two key advancements.

(1) Incorporation of additional disturbances: Recognizing the limitations of previous studies that did not fully account for environmental factors, this study integrates the receiver's bow wave effect and wind turbulence. These disturbances are crucial in understanding the real-world dynamics of drogue systems.

(2) Utilization of numerical simulations: Identifying the costly and resource-intensive nature of experimental methods, this study employs numerical simulations to provide a more comprehensive study. This approach not only avoids high costs associated with extensive experimental setups but also allows for a detailed and comprehensive analysis. By integrating numerical simulations, this study complements and significantly extends the experimental findings of Ro et al. This enables a broader exploration of scenarios and conditions, which might be impractical or prohibitively expensive to replicate experimentally, thereby enriching our understanding of actively stabilized drogues.

By addressing these aspects, the current research not only fills a critical gap in the field but also enhances the understanding of actively stabilized drogues, offering insights that are essential for the development of active stabilized drogue systems.

This study employs an actively stabilized drogue system with four controllable control surfaces to mitigate the impact of bow wave perturbations on aerial refueling operations. Additionally, as part of the research objective, the study aims to develop an active stabilization drogue model using MATLAB Simulink, while considering wind turbulence and the bow wave effect.

A mathematical model of the hose-drogue system is utilized to analyze the resultant disturbance forces and the system's oscillations due to bow wave effects on a specific fighter jet. The system's aerodynamic characteristics are determined through aerodynamic simulations, and subsequent analysis involved fitting the data using a combination of a linear aerodynamics model and polynomials. A linear quadratic regulator (LQR) controller is developed

that can be applied to the control surfaces of the actively stabilized drogue system. The study evaluates the system's effectiveness against bow wave disturbances using a MATLAB Simulink environment that implements a hose-drogue model. The objective of this study is to improve the safety and stability of aerial refueling operations by assessing the actively stabilized drogue system's performance against bow wave perturbations. Numerical simulations are conducted to investigate the impact of various control surface deflection angles on the aerodynamic behavior of a hose-drogue system. Specifically, the study aims to examine the interaction between aerodynamic disturbances and hose catenaries. Overall, the simulation results reveal that the actively controlled drogue significantly reduces the displacement of the hose, thereby improving the system's performance against bow wave perturbations.

## 1 Modeling of Hose-Drogue System

### 1.1 Definition of coordinate system

In order to establish a mathematical model of the hose-drogue system, an inertial coordinate system ( $O_T, X_T, Y_T, Z_T$ ) is established with its  $X$ -axis oriented opposite to the direction of the tanker aircraft,  $Y$ -axis as the vertical axis pointing upward, and  $Z$ -axis determined by the right-hand rule. A modeling reference frame ( $O_P, X_P, Y_P, Z_P$ ), parallel to the inertial coordinate system, is defined with  $O_P$  located at the junction between the hose and the refueling pod (towed point). Additionally, a drogue coordinate system ( $O_D, X_D, Y_D, Z_D$ ) is established at the connecting point between the hose and drogue as shown in Fig.1. Each small section of the  $i$ th segment of the hose can be described by two relative Euler angles  $\theta_{i,1}$  and  $\theta_{i,2}$ , relative to the modeling reference frame. Finally, a receiver aircraft coordinate frame ( $O_R, X_R, Y_R, Z_R$ ) is established at the refueling probe of the receiver aircraft, parallel to the inertial coordinate system. A schematic representation of the coordinate axes is depicted in Fig.1.

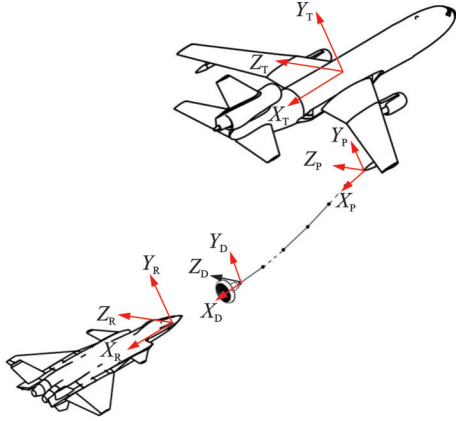


Fig.1 Definition of coordinate systems

## 1.2 Modeling description

This study employs multi-rigid body dynamics to develop a mathematical model of the hose-drogue system. The model decomposes the system into interconnected segments, whereby the hose comprises a finite number of cylindrical rods connected by joints (nodes), and the drogue is considered a lumped mass. The mathematical model allows for analysis and computation of the system's dynamic behavior, providing insights into the kinematics and dynamics of the system. The mathematical model underlying the hose drogue system is illustrated in Fig.2. Furthermore, the system is simplified by neglecting axial elongation and torsion of the hose, allowing the application of the proposed method to the system for further investigation.

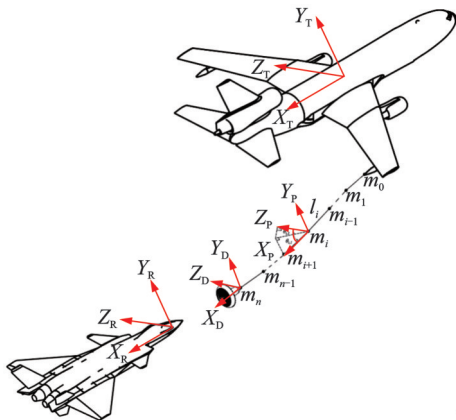


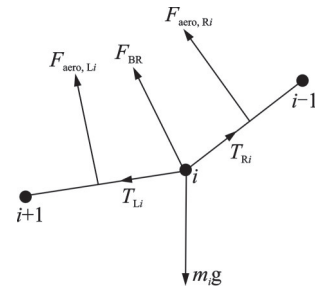
Fig.2 Description of hose multi-body system model and coordinate system

The hose system is labelled by assigning numbers to its nodes and hose segments. The node num-

bering starts from 0, which is located at the refueling pod, and increases sequentially up to  $n$ , which is located at the refueling drogue. The hose section numbering increases sequentially from 1 to  $n$ . The length of each small segment  $i$  is denoted as  $l_i$ .

## 1.3 Force analysis on the nodes

Force analysis is conducted on each node. Each node has external forces acting on it, including tension forces from the left and right hose segments (indicated by subscripts L and R, respectively), gravitational force, aerodynamic forces, and force of the hose bending restoring force. Taking  $i$  as an example, the external forces acting on the node are shown in Fig.3, along with an associated lumped mass  $m_i$ .

Fig.3 Force analysis of node  $i$ 

The mass of each node is defined as

$$m_i = \begin{cases} \frac{(l_i + l_{i+1})\rho_{\text{hose}}}{2} & i = 1, 2, \dots, n-1 \\ \frac{l_i\rho_{\text{hose}}}{2} + m_{\text{drogue}} & i = n \end{cases} \quad (1)$$

where  $\rho_{\text{hose}}$  represents the linear density of the hose, and  $m_{\text{drogue}}$  the mass of the drogue.

The aerodynamic forces exerted on the system can be divided into three components: Drogue drag, frictional drag and pressure drag.

$$D_{\text{drogue}} = \frac{1}{2} \rho v^2 S C_{d,\text{dro}} \quad (2)$$

$$D_{\text{skf}} = \frac{1}{2} \rho v^2 \pi d_o l C_f \quad (3)$$

$$D_{\text{press}} = \frac{1}{2} \rho v_n^2 d_o C_d \quad (4)$$

where  $S$  represents the drogue canopy area;  $\rho$  the air density;  $d_o$  the outer diameter of the hose;  $C_{d,\text{dro}}$ ,  $C_f$ , and  $C_d$  represent the drogue drag coefficient, skin friction drag coefficient, and pressure drag coefficient, respectively. Additionally, the tangential

and normal velocities are denoted as  $v_t$  and  $v_n$ , respectively.

The bending restoring force can be expressed as

$$F_{BR} = \frac{8EI}{|L_L + L_R|^2} \left( \arccos \left( \frac{L_L \cdot (L_L + L_R)}{|L_L| |L_L + L_R|} \right) + \arccos \left( \frac{L_R \cdot (L_L + L_R)}{|L_R| |L_L + L_R|} \right) \right) \quad (5)$$

where  $L$  is the position vector between the  $i$ th node and left or right node (indicated by the subscript of L or R, respectively),  $I$  the moment of inertia of the hose segment, and  $E$  the Young's modulus of the hose.

Thus, the total external force  $F_i^{\text{ext}}$  acting on the node can be expressed as

$$F_i^{\text{ext}} = \begin{cases} \frac{F_{\text{aero},Li} + F_{\text{aero},Ri}}{2} + F_{BR} + m_i g & i = 1, 2, \dots, n-1 \\ \frac{F_{\text{aero},Li}}{2} + m_i g + D_{\text{drogue}} & i = n \end{cases} \quad (6)$$

By applying Newton's second law  $F = ma$ , the acceleration of the node  $a_i$  can be defined as

$$a_i = \begin{cases} \frac{F_i^{\text{ext}} + T_{Li} + T_{Ri}}{m_i} & i = 1, 2, \dots, n-1 \\ \frac{F_i^{\text{ext}} + T_{Ri}}{m_n} & i = n \end{cases} \quad (7)$$

To determine the tension force, it is assumed that the hose is inextensible and of constant length. The relationship between the position vector of a segment and hose length can be expressed as

$$r_i^2 = l_i^2 \quad (8)$$

where  $r_i$  represents the position vector of hose segment  $i$  and  $l_i$  the length of hose segment  $i$ .

By differentiating Eq.(8) with respect to time twice, the acceleration constraints equations can be obtained as

$$(a_i - a_{i-1})r_i + r_i^2 = \dot{l}_i^2 + l_i \ddot{l}_i \quad (9)$$

The tension at node  $i$ ,  $T_i$ , is a function of the force magnitude  $t_i$  and direction represented by the unit vector  $n_i$  pointing from node  $i-1$  to node  $i$ . A positive value of  $t_i$  indicates tensile force while a negative value infers a compressive force acting on the node.

$$T_i = t_i n_i \quad (10)$$

The linear algebraic equation for the tension of the hose segments can be obtained by substituting Eq.(7) into Eq.(9).

After establishing the boundary conditions, including the location of the towed point, and the drogue connecting point, the dynamic equations for each node of the hose can be written in the matrix form of  $A_{N \times N} T_{N \times 1} = B_{N \times 1}$ , which can be solved using numerical methods such as the Thomas algorithm to accelerate convergence.

#### 1.4 Kinematic equations

Suppose the nodes  $i$  and  $i-1$  are associated with position vectors  $p_i$  and  $p_{i-1}$ , respectively, in the  $O_P, X_P, Y_P, Z_P$  coordinate system. The relationship between the spatial position vector and the  $i$ th segment can be expressed as

$$r_i = p_i - p_{i-1} \quad (11)$$

Taking the first- and second-order derivatives of the position vector yields the velocity and acceleration shown as

$$\dot{r}_i = v_i - v_{i-1} = \sum_{k=1}^2 r_{i,\theta_{i,k}} \dot{\theta}_{i,k} + r_{i,l} \dot{l}_i \quad (12)$$

$$\ddot{r}_i = a_i - a_{i-1} = \sum_{k=1}^2 (\ddot{r}_{i,\theta_{i,k}} \ddot{\theta}_{i,k} + \dot{r}_{i,\theta_{i,k}} \dot{\theta}_{i,k}) + r_{i,l} \ddot{l}_i + \dot{r}_{i,l} \dot{l}_i \quad (13)$$

where the partial derivatives of the position vector are described as

$$\frac{\partial r_i}{\partial \theta_{i,k}} = r_{i,\theta_{i,k}} \quad (k=1,2), \quad \frac{\partial r_i}{\partial l_i} = r_{i,l} \quad (14)$$

Then, by multiply  $r_{i,\theta_{i,j}}$  ( $j=1,2$ ) on both sides of Eqs.(12) and (13),  $r_{i,\theta_{i,j}} \cdot r_{i,\theta_{i,j}} = 0$  yields the angular acceleration shown as

$$\ddot{\theta}_{i,j} = \frac{-r_{i,\theta_{i,j}} \left( \sum_{k=1}^2 \dot{r}_{i,\theta_{i,k}} \dot{\theta}_{i,k} + r_{i,l} \ddot{l}_i + \dot{r}_{i,l} \dot{l}_i - a_i + a_{i-1} \right)}{|r_{i,\theta_{i,j}}|} \quad j=1,2 \quad (15)$$

By knowing the velocities and accelerations of both the towed point and every node in the hose, the orientation angle  $\theta_{i,k}$  and its first derivative for each section of the hose can be approximated utilizing the fourth-order Runge-Kutta method for the equation above.

To ensure an accurate investigation of the drogue's behavior, it is inadequate to model it as a

point mass without considering the variations in its attitude. Therefore, proper consideration of the drogue's attitude variations is necessary. Assuming the absence of rolling motion on the drogue, its orientation can be determined solely by its pitch and yaw. The pitching and yawing moments are defined in the  $O_T, X_T, Y_T, Z_T$  coordinate system as follows

$$\mathbf{M}_{\text{pitch}} = m_{\text{drogue}} g l_{\text{cg}}^n + \mathbf{M}_{\text{pitch}}^{\text{drogue}} \quad (16)$$

$$\mathbf{M}_{\text{yaw}} = \mathbf{M}_{\text{yaw}}^{\text{drogue}} \quad (17)$$

The notation  $l_{\text{cg}}^n$  denotes the distance between the position of the drogue's centre of gravity and the hose end. By using Eq.(18), the angular acceleration of the drogue is obtained as

$$\ddot{\theta}_{d,k} = \frac{M}{\mathbf{I}_{\text{drogue}}^R} \quad (18)$$

where  $\mathbf{I}_{\text{drogue}}^R$  represents the moment of inertia of the drogue after performing coordinate transformations.

### 1.5 Modeling of bow wave effect

During the docking phase, disturbances are induced by the receiver aircraft by altering the flow field around the drogue body. The disturbance input in this study is defined as the angle between the wind velocity vector and the inertial reference frame. The disturbance can be considered as a change in the drogue's orientation to the wind direction. The wind velocity vector  $\mathbf{v}_w$  is then transformed into the inertial reference frame using a transformation matrix  $L_w^R$ . The disturbed wind velocity vector  $\mathbf{v}$ , represented in Eq.(19), is the difference between the transformed wind velocity vector and the drogue velocity vector. Eqs.(20) and (21) specify the azimuth angle of the wind axes relative to the inertial axes.

$$\mathbf{v} = \begin{pmatrix} v_x \\ v_y \\ v_z \end{pmatrix} = L_w^R \mathbf{v}_w - \mathbf{v}_{\text{drogue}} \quad (19)$$

$$\theta_{r,1}^w = \arcsin \frac{v_z}{\|\mathbf{v}\|} \quad (20)$$

$$\theta_{r,2}^w = \arctan \frac{v_y}{v_x} \quad (21)$$

### 1.6 Modeling of turbulence

This study utilizes the Dryden wind turbulence model<sup>[10-11]</sup> to simulate moderate turbulence levels that are proportional to the expected wind turbu-

lence at a given altitude and airspeed. The model utilizes the Dryden spectral representation to introduce turbulence by adding band-limited white noise. The study only considers the lateral and vertical turbulences in the spectral functions and components, while the longitudinal component is not included. The MIL-F-8785C specification provides spectral functions, represented by Eqs.(22) and (23), used to calculate the turbulence energy distribution for the lateral and vertical component spectra functions in the Dryden wind turbulence model. The model generates a three-dimensional wind turbulence velocity vector, which is then superimposed onto the wind velocity vector  $\mathbf{v}_w$ . By superimposing the turbulence velocity on the wind velocity, the model can account for the influence of turbulence on the overall flow field, ultimately affecting the drogue's overall aerodynamic behavior.

$$\text{Lateral: } \Phi_v(\omega) = \frac{\sigma_v^2 L_v}{\pi V} \cdot \frac{1 + 3 \left( L_v \frac{\omega}{V} \right)^2}{\left[ 1 + \left( L_v \frac{\omega}{V} \right)^2 \right]^2} \quad (22)$$

$$\text{Vertical: } \Phi_w(\omega) = \frac{\sigma_w^2 L_w}{\pi V} \cdot \frac{1 + 3 \left( L_w \frac{\omega}{V} \right)^2}{\left[ 1 + \left( L_w \frac{\omega}{V} \right)^2 \right]^2} \quad (23)$$

where  $\omega = V\Omega$  relates the circular frequency ( $\omega$ ) of a fluid to its airspeed ( $V$ ) and spatial frequency ( $\Omega$ ), and the turbulence scale lengths and intensities are represented by  $L_u, L_v, L_w$  and  $\sigma_u, \sigma_v, \sigma_w$ , respectively.

### 1.7 Model validation for hose-drogue system

To validate the accuracy of the mathematical model of the hose-drogue, numerical simulations are conducted using the settings from Ref.[4] and the results (Dimensionless drogue vertical position, DDVP) are compared to the values obtained from the same reference. The DDVP is a dimensionless parameter introduced by Ref.[2] and defined as  $V_D/L_H$ . Here  $V_D$  represents the vertical distance between the connecting point of the hose and drogue and the towed point, and  $L_H$  the straight-line distance from the towed point to the hose and drogue

coupling. In the simulations, a uniform flow is utilized as the flow field to simplify the calculation procedure, since the reference shows that F/A-18A tanker's wake has little effect on the steady-state trailing hose. Flow data and characteristics of the hose-drogue assembly are sourced from the same comparative material. The results indicate that good agreement is achieved between the calculated and comparative data, thereby confirming the robustness of the mathematical model utilized.

This study is conducted at two different flight altitudes of 2 286 m (7 500 ft) and 7 620 m (25 000 ft) over the airspeed range from 87.5 m/s (170 kts) to 159.5 m/s (310 kts).

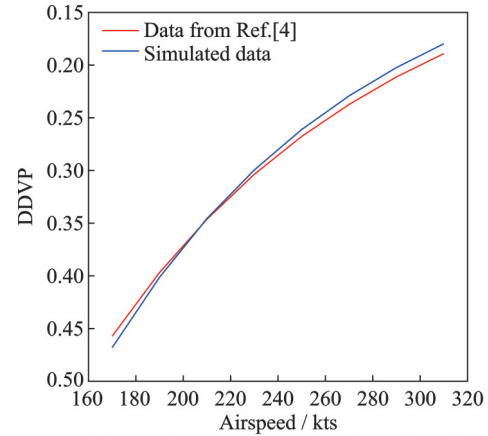
Table 1 presents the DDVP and its respective deviation ( $\Delta$ ) compared to the reference source<sup>[4]</sup>. The information is graphically displayed in Fig.4(a). The analysis finds that the percentage deviation observed at low airspeed conditions could be attributed to the effect of the F/A-18A tanker's wake. In this study, a model based on steady or uniform flow is used, which differs from the methodology used in the reference source.

**Table 1 Computed DDVP and its percentage of deviation**

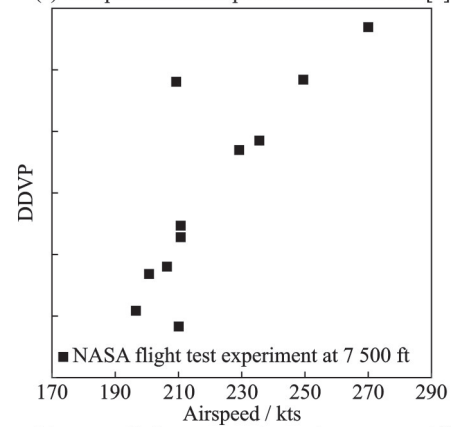
Airspeed/ kts	Altitude/ ft			
	7 500		25 000	
	DDVP	$\Delta$ /%	DDVP	$\Delta$ /%
170	0.468 1	+2.38	0.652 0	+4.42
190	0.401 3	+1.12	0.581 1	+3.96
210	0.345 6	-0.18	0.516 5	+3.12
230	0.299 5	-1.33	0.459 3	+2.19
250	0.261 1	-2.48	0.409 3	+1.29
270	0.229 2	-3.41	0.365 6	+0.32
290	0.202 3	-4.22	0.327 7	-0.60
310	0.179 7	-4.94	0.294 6	-1.50

Additionally, the results are compared with data obtained from a flight test conducted by the national aeronautics and space administration (NASA). The trend displayed in the computed results matches well with the flight-test results presented in Ref.[2], which is represented in Fig.4(b). This provides further validation of the numerical simulation and confirmed the accuracy of the mathematical model used in this study. The findings support the reliability of the research and provide evi-

dence to suggest that the steady-state drogue position problem can be effectively analyzed using the mathematical model under given conditions.



(a) Comparison of computed results with Ref.[4]



(b) NASA flight test experiment data at 7 500 ft<sup>[2]</sup>

Fig.4 Comparison of results with references

## 1.8 Numerical simulation of the bow wave effect

### 1.8.1 Neighboring cell search algorithm

In order to calculate the forces acting on the hose-drogue system, it is required to obtain the flow field parameters such as velocity and density. Nevertheless, locating the position of a drogue in a flow field and acquiring the flow field parameters can become computationally expensive due to the high number of grid counts. To address this issue, a neighboring cell search algorithm has been proposed in prior studies<sup>[12-13]</sup>, which utilizes the adjacency information of unstructured grids to facilitate the rapid determination of desired location.

The specific steps involved in the searching process on an unstructured tetrahedral mesh are

- (1) Select a cell as the initial cell, such that it avoids the boundary of the object and accelerates the process if the starting cell is closer to the target.

(2) Let the current loop be  $i$ , and the current cell with the coordinates of  $(X_{in}, Y_{in}, Z_{in})$  its centroid.

(3) Evaluate the equation of a plane for each face  $j$  of the current cell, the general equation of its plane can be expressed as

$$A_j x + B_j y + C_j z + D_j = 0$$

(4) Substitute the centroid and drogue coordinates into the plane equation to determine whether the cells are on the same or opposite side of the plane. If the current cell and target point are on the opposite side of the plane, continue searching for the neighboring cell until a cell consisting of all faces that are on the same side of the plane, and use that cell as the initial cell for the next time step.

### 1.8.2 Bow wave simulation method and results

This study investigates the effects of the bow wave effect on the hose-drogue system. The procedure is as follows:

(1) Establish the mesh of the aircraft then use CFD to calculate all parameters of the uniform flow field of the receiver aircraft.

(2) The steady-state position computed from the mathematical model of the hose-drogue system is used as the initial value for the hose and drogue.

(3) The neighboring cell search algorithm is used to obtain the flow field parameters for force calculations. The position, relative angle, and forces acting on the hose are initialized, and the force on each node of the hose-drogue is calculated and mapped onto the established hose-drogue model.

(4) Based on the established mathematical model of the hose segment, the velocity of each segment is determined, and the distance moved by the hose-drogue model in the given time interval is calculated based on the docking velocity of the receiver aircraft and the time interval. The moving distance is then mapped onto the grid nodes, and the process is iterated until the docking is complete.

The disturbance force acting on the drogue is illustrated in Fig.5. During the initial docking stage when the receiver aircraft is 10 m away from the drogue, the disturbance is observed to be insignificant. However, once the distance between the aircraft head and the drogue decreases to 2.5 m, at approximately 15 s, the disturbance force acting on the drogue increases drastically. This drastic in-

crease in disturbance force is attributed to changes in the aircraft flow field, specifically, the pressure and velocity around the aircraft's nose where the drogue is located. These changes in the flow field result in the significant rise in disturbance force experienced by the drogue.

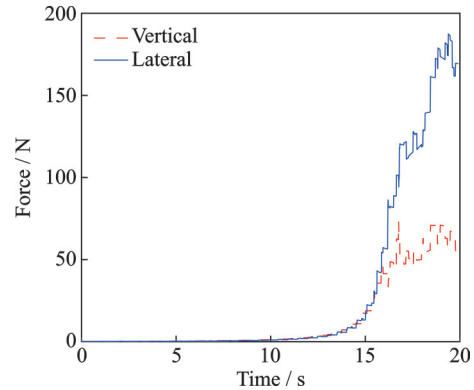


Fig.5 Forces acting on the drogue due to the bow wave effect of the receiver aircraft

Fig.6 shows the motion trajectory of the drogue in the  $YZ$  plane. It can be observed that the disturbance force caused by the bow wave effect pushes the drogue away from the refueling probe, resulting in an upward and outward swinging motion. Eventually, the drogue stabilizes in the upper left side of its initial position, where it undergoes irregular oscillations.

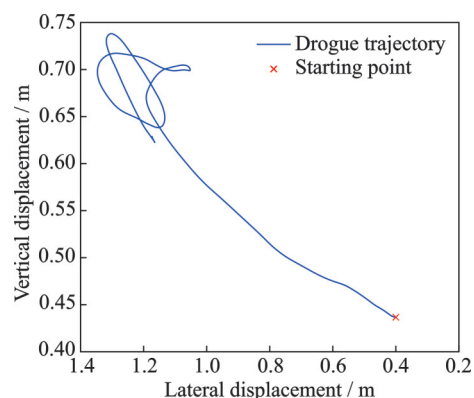


Fig.6 Drogue's motion trajectory in the presence of bow wave effect

## 2 Design of an Actively Controllable Stabilizing Drogue

### 2.1 Challenges of drogue behavior during approach

The previous chapter shows that the bow wave

effect can push the drogue away when the refueling probe is approaching, resulting in challenges during mid-air refueling operations. As a result of these observations, pilots are trained to anticipate the movement of the drogue instead of reacting to it randomly. Therefore, the outcome of aerial refueling maneuvers is greatly dependent on the pilot's sharp judgment, exceptional skill, and extensive experience in anticipating and responding to the drogue's movements. The development of actively controllable stabilizing drogue technology helps to address these challenges by providing a more stable target for pilots during aerial refueling operations. This technology reduces risks and improves the accuracy of aerial refueling operations, enabling pilots to carry out the mission successfully.

## 2.2 Structural design of actively controllable stabilizing drogue

This study introduces an actively controllable stabilizing drogue design based on the experimental work of Ref.[6]. However, their study lacked theoretical modeling and simulation. This limitation is addressed by providing a mathematical model and simulation for the design. Furthermore, considering performing wind tunnel testing is cost extensive, the study presents a cost-efficient alternative to validate the performance analysis through computer simulation. The drogue features four NACA0024 symmetrical control surfaces attached to the traditional drogue in a plus (+) configuration, including two pairs of opposing wing-shaped structures installed on the left, right, top, and bottom of the drogue. The design of the control surface is designed with a length shorter than the drogue diameter. This specific design choice is made to ensure that the control surface can be conveniently stowed when not in use. It is important to note that this design is purely conceptual and does not include a joint. These surfaces are rotated by servo motors that allow independent and non-interfering movement. The presence of multiple control surfaces enhances stabilization and improves control efficiency. The schematic diagram of the drogue design is presented in Fig.7.

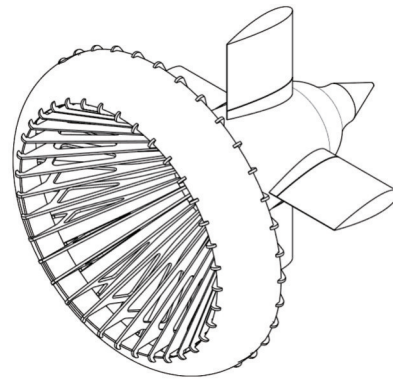


Fig.7 Design of actively controllable drogue

## 3 Simulation of Aerodynamic Characteristic

### 3.1 Modeling and simulation of active controllable stabilizing drogue

This study uses CATIA V5, a 3D CAD modelling software, to model the active controllable stabilizing drogue. The model is then imported into ANSYS ICEM CFD, a commercial meshing software, to generate an Octree unstructured mesh. An unstructured mesh is chosen due to the complex geometry of the drogue. CFD simulations are conducted to analyze the aerodynamic characteristics of the drogue using the Spalart-Allmaras one-equation turbulence model<sup>[14]</sup>. The Spalart-Allmaras model is known to be superior in aerospace applications<sup>[15]</sup>. ANSYS Fluent, a commercial CFD solver, is used to conduct the simulations. The altitude used in this study is 6 km, with a Mach number of 0.562 7. During the simulations, only the horizontal control surfaces are deflected, while the vertical control surface remains stationary. This is done to reduce the computational time and resources required for the analysis, based on the assumption that the symmetrical geometry of the two control surfaces would lead to similar behaviour. However, it is important to note that if the vertical control surfaces behave differently than expected, the accuracy of results could be impacted.

### 3.2 Aerodynamic data analysis

The aerodynamic data obtained from CFD calculations is further simplified using curve fitting techniques, including linear interpolation and polynomial fitting. This process uses the drogue angle of

attack (AOA), angle of sideslip (AOSS), and control surface deflection angle  $u_1$  to determine aerodynamic parameters. The collected data assumes a valid range of drogue's AOA within  $-5^\circ$  to  $5^\circ$ . Linear interpolation is used to obtain additional data points within this range based on the drogue's AOA and AOSS.

Fig.8 depicts the correlation between lift, AOA, AOSS, and control input. Fig.8(a) shows the dependence of lift on drogue AOA and AOSS. The results demonstrate that the drogue AOA has a more significant impact than AOSS, which has a negligible effect. Fig.8(b) reveals the effect of changing the deflection angle of the horizontal control surface ( $u_1$ ) on the lift coefficient. The results demonstrate a proportional relationship between the deflection angle and lift coefficient. Fig.9 shows the correlation between lateral force, AOA, AOSS, and control input. Fig.9(a) shows the lateral force as a function of AOSS and AOA of the drogue, indicating that the AOSS is the primary factor affecting the lateral force. Meanwhile, Fig.9(b) illus-

trates the effect of deflecting the horizontal control surface on the lateral force coefficient. Fig.10 presents the results of active stabilizing drogue drag characteristics. Fig.10(a) shows the dependence of drag on the drogue's AOA and AOSS, showing that low values of drogue's AOA and AOSS have minimal impact on drag. The primary reason is that the wing's deflection angle compensates for the drag reduction caused by the drogue's AOA and AOSS. Fig.10(b) shows the effect of changing the horizontal control surface deflection angle on the drag coefficient. Fig.11 and Fig.12 show the results of pitching moment and yawing moment of the drogue, respectively. The left figure shows the calculated moment in the node coordinate system, which is parallel to the modeling reference system ( $O_p, X_p, Y_p, Z_p$ ). The right figure shows the calculated moment in parallel to the modeling coordinate system. This represents the effect of the deflection angle of the horizontal control surface on the coefficients of the yawing and pitching moments. The results show that the horizontal control surface deflection has a curvi-

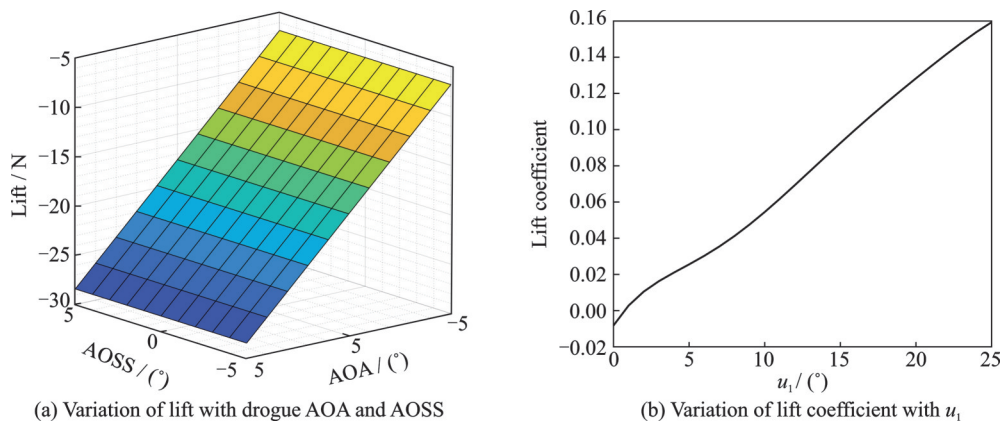


Fig.8 Correlation between lift, AOA, AOSS, and control input

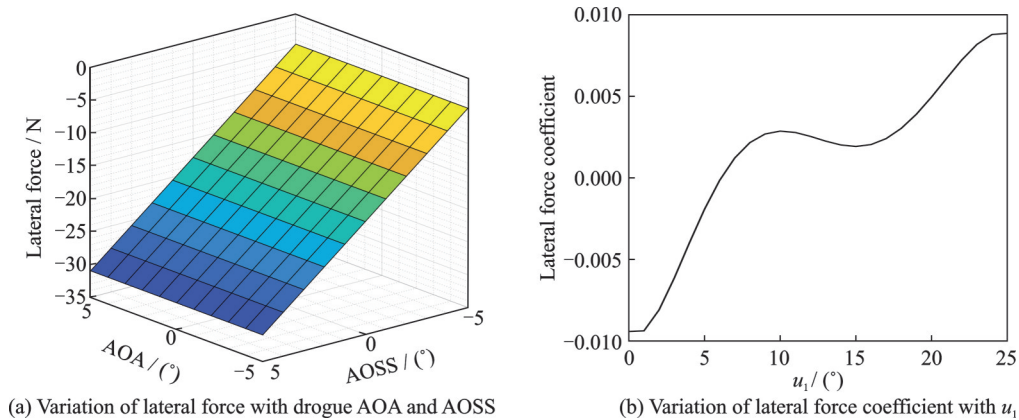


Fig.9 Correlation between lateral force, AOA, AOSS, and control input

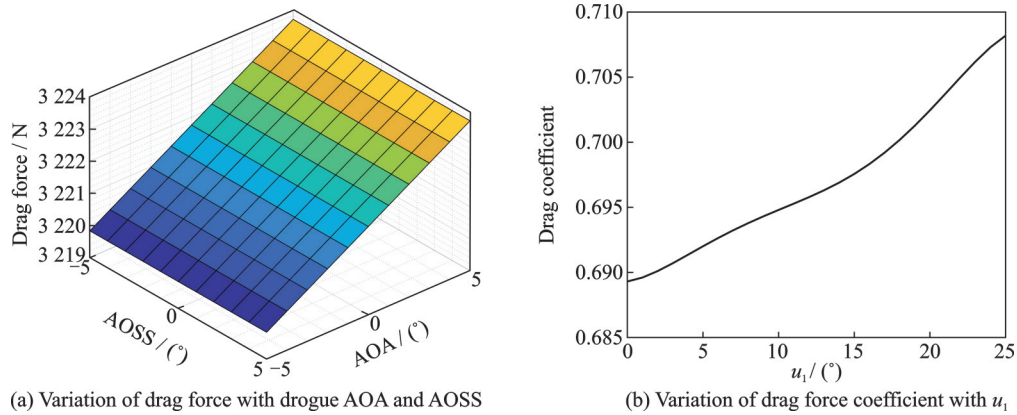


Fig.10 Correlation between drag force, AOA, AOSS, and control input

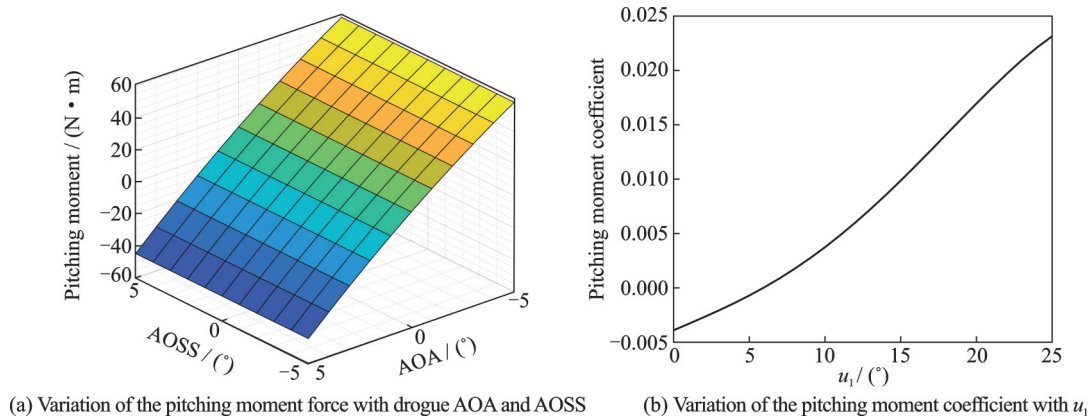


Fig.11 Correlation between pitching moment, AOA, AOSS, and control input

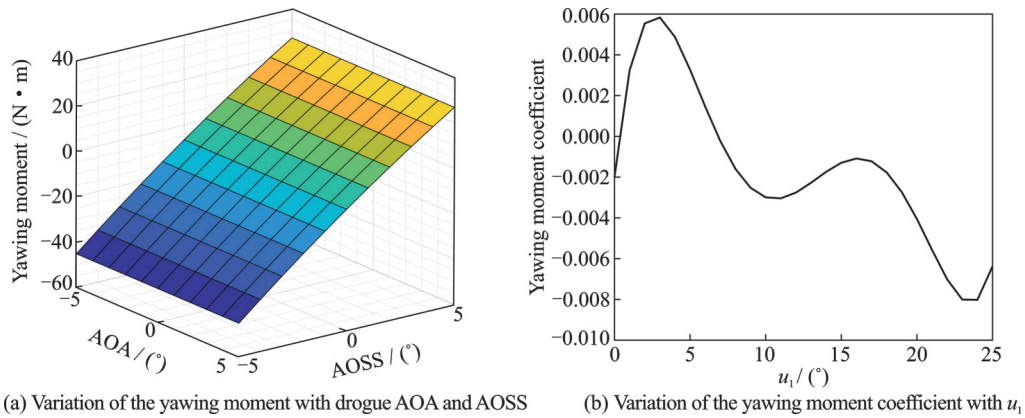


Fig.12 Correlation between yawing moment, AOA, AOSS, and control input

linear relationship with the pitching moment, with only a wavy correlation to the yawing moment.

### 3.3 Aerodynamic model

By simplifying the aerodynamic database obtained from the CFD simulations of the active stabilizing drogue and establishing an aerodynamic model, the control force on the drogue can be directly obtained by measuring the drogue's attitude and flight environment information.

The aerodynamic model, represented by Eq.

(29), divides the aerodynamic force acting on the drogue into three parts: The initial state of the drogue, the attitude of the drogue, and the attitude of the control surfaces.

$C_0$  in the model represents the baseline aerodynamic parameters of the drogue in its initial state. To account for the moment generated by gravity, the drogue is assumed to maintain an AOA of  $\alpha_0 = 2.6^\circ$ . This balances the corresponding moment generated by gravity, and the selection of this angle is

based on the simulation results. The AOA will create an aerodynamic force in the opposite direction of the gravitational force, which will produce a moment that offsets the moment created by gravity.  $C_\alpha$  and  $C_\beta$  represent the derivative vectors of the aerodynamic parameters corresponding to the drogue's AOA,  $\alpha$  and AOSS,  $\beta$ , respectively.  $C_{u_i}$  represents the vector of the aerodynamic parameter corresponding to the deflection of the control surface against matrix  $u_1$ .

A fitted polynomial function is used to estimate the drag coefficient for the control surfaces based on the lift coefficient. The polynomial function is fitted onto the plot of drag coefficient versus lift coefficient and allowed for the more precise estimation of the drag coefficient for a given lift coefficient. The use of the fitted polynomial function provides an efficient way to estimate the drogue's aerodynamic characteristics, making it easier to predict its behavior and performance in different operational scenarios.

Finally, the aerodynamic forces and moments caused by the control surface are converted from the local coordinate system into the global coordinate system. By fitting the polynomial function onto the plot of drag coefficient versus lift coefficient, it becomes possible to estimate the drag coefficient for a given lift coefficient value. Using the coordinate transformation  $L_A^r$  to convert the force and moment generated by the control surface in its local coordinate system to the drogue coordinate system.

$$C_0 = [C_{D0} \ C_{L0} \ C_{Y0} \ C_{my0} \ C_{mp0}]^T \quad (24)$$

$$C_\alpha = [C_{D\alpha} \ C_{L\alpha} \ C_{Y\alpha} \ C_{my\alpha} \ C_{m\beta\alpha}]^T \quad (25)$$

$$C_\beta = [C_{D\beta} \ C_{L\beta} \ C_{Y\beta} \ C_{my\beta} \ C_{m\beta\beta}]^T \quad (26)$$

$$C_{u_i} = [C_{Du_i} \ C_{Lu_i} \ C_{Yu_i} \ C_{myu_i} \ C_{mpu_i}]^T \quad (27)$$

$$u_1 = \begin{bmatrix} u_1^2 & 0 & 0 & 0 & 0 \\ 0 & u_1 & 0 & 0 & 0 \\ 0 & 0 & u_1 & 0 & 0 \\ 0 & 0 & 0 & u_1 & 0 \\ 0 & 0 & 0 & 0 & u_1 \end{bmatrix} \quad (28)$$

$$\begin{bmatrix} F_{aero} \\ M_{aero} \end{bmatrix} \approx qL_w^r \left( C_0 + [C_\alpha \ C_\beta] \begin{bmatrix} \alpha - \alpha_0 \\ \beta \end{bmatrix} + u_1 L_A^r C_{u_i} \right) \quad (29)$$

Tables 2—5 present the aerodynamic parameters for the actively stabilizing drogue.

**Table 2 Coefficients of the baseline parameters of drogue**

Parameter	Value
$C_{D0}$	1.384 734
$C_{L0}$	0.009 976
$C_{Y0}$	0
$C_{my0}$	0
$C_{m\beta0}$	0.009 982

**Table 3 Mean coefficient change with respect to 1° of AOA increment**

Parameter	Value
$C_{D\alpha}$	0
$C_{L\alpha}$	0.000 6119
$C_{Y\alpha}$	0
$C_{my\alpha}$	0
$C_{m\beta\alpha}$	-0.004 058

**Table 4 Mean coefficient change with respect to 1° of AOSS increment**

Parameter	Value
$C_{D\beta}$	0
$C_{L\beta}$	0
$C_{Y\beta}$	0.000 611 9
$C_{my\beta}$	0.004 058
$C_{m\beta\beta}$	0

**Table 5 Mean coefficient change with respect to 1° of deflection angle of horizontal control surface**

Parameter	Value
$C_{Lu_i}$	0.006 792
$C_{Yu_i}$	0
$C_{myu_i}$	0
$C_{mpu_i}$	0.001 225

## 4 Modeling of Control Systems Through Simulation

Numerical simulations are employed to update the aerodynamic database. The simulations involve substituting the drogue and control surface attitude into the aerodynamic model to compute control forces. These forces are then fed into a nonlinear simulation of the hose-drogue system to evaluate the actively controllable stabilizing drogue's disturbance resistance and its ability to suppress oscillations. Table 6 shows various parameters for the hose and drogue.

**Table 6 Components and configurations of hose and drogue**

Component	Configuration	
	Parameter	Value
Hose	Length/m	22.5
	Linear density/(kg·m <sup>-1</sup> )	2.38
	Diameter (inner)/mm	50.8
	Diameter (outer)/mm	67.3
	Young's modulus/10 <sup>7</sup> Pa	1.379
Drogue	Mass/kg	30
	Canopy area/m <sup>2</sup>	0.468
	$I_{xx}$	0.8
	$I_{yy}$	1.105 7
	$I_{zz}$	1.105 7
	Control surface reference area/m <sup>2</sup>	0.222 5
Hose with fuel	Linear density/(kg·m <sup>-1</sup> )	4.205

#### 4.1 Design of LQR control system

The system design employs a LQR controller, which plays a critical role in maintaining the relative position between a drogue and tanker aircraft. This is achieved through the control forces generated by deflecting the control surfaces.

A key advantage of employing the LQR controller in system design is its efficiency in energy usage. This attribute is particularly significant when compared with other control strategies like proportional integral derivative (PID) or fuzzy controllers<sup>[16]</sup>. The LQR's ability to optimally balance state error and control effort translates into a more judicious use of energy, making it an excellent choice for energy-efficiently demanding systems. Increased energy efficiency naturally leads to lower power consumption, especially in battery-dependent applications. As a direct consequence, systems controlled by a LQR exhibit increased endurance, capable of operating for extended periods without frequent recharging or battery replacement. This makes the LQR an invaluable tool in scenarios where prolonged operational capability and sustainability are critical considerations. Thus, the selection of LQR is not only based on its ability to effectively control the position but also on its contribution to enhancing the overall endurance and feasibility of prolonged aerial refueling operations.

The system aims to suppress the drogue's angular velocity and acceleration while simultaneously ensuring that the prescribed AOA and AOSS are

maintained. The system is designed to stabilize the drogue in its set position during aerial refueling operations. Furthermore, the LQR is recognized as an optimal control solution that not only offers robust performance but also excels in maintaining minimal steady-state errors<sup>[17]</sup>.

The dynamic and static pressure ports installed on the drogue provide measurements of the surrounding air pressure, which are used to determine the actual atmospheric conditions surrounding the drogue.

Various parameters of the drogue's motion, such as attitude, velocity, acceleration, angular velocity, and angular acceleration, could be measured by employing a combination of sensors, such as GPS and the inertial measurement unit (IMU).

Additionally, a differential global positioning system (DGPS) or photogrammetry could be used to determine the drogue's position and deviation from the setpoint. Fig.13 demonstrates the block diagram of the LQR controller system.

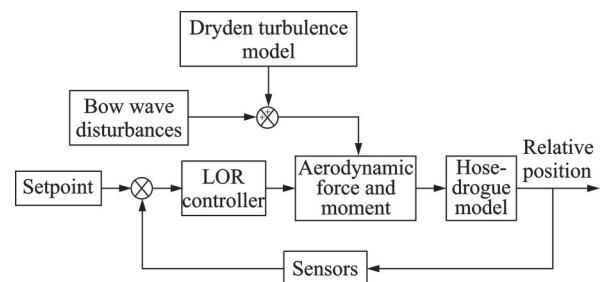


Fig.13 Block diagram of LQR controller system for hose-drogue model

An important assumption in the design of the LQR controller is that it operates under the premise of precise and noise-free measurements. This assumption is critical for the optimal performance of the controller, as it relies on accurate data to select control inputs that track the desired state while maintaining system stability.

Eqs.(30, 31) represent the cost function and state equations for the hose-drogue system. An LQR controller is a full-state feedback controller, which is designed to achieve optimal control of the dynamic system by minimizing the cost function while also minimizing power consumption. The controller selects control inputs that track the desired state while keeping the system stable, achieving the

desired control objectives while conserving power.

The control vector, denoted by Eq.(32), represents the deflection angles of two servo actuators used to control the horizontal and vertical deflection of the control surfaces.

$$J = \int_0^{20} (\mathbf{x}^T \mathbf{Q} \mathbf{x} + \mathbf{B}^T \mathbf{R} \mathbf{u}) dt \quad (30)$$

$$\dot{\mathbf{x}} = \mathbf{A} \mathbf{x} + \mathbf{B} \mathbf{u} \quad (31)$$

$$\mathbf{u} = [u_1 \quad u_2]^T \quad (32)$$

Eq.(33) represents a state vector, which includes the state variables required to describe the position error between the coordinates in the inertial system and a reference point. Since the length of the hose remains constant, only the  $YZ$  plane coordinates of the drogue are needed to describe the position of the hose-drogue system. In addition to the position error, the state variables include the oscillation velocities, AOA, AOSS, pitch moment, and yaw moment of the drogue in both the vertical and horizontal directions relative to the inertial system.

$$\mathbf{x} = \begin{bmatrix} y \\ z \\ v_y \\ v_z \\ \alpha \\ \beta \\ v_{\omega z} \\ v_{\omega y} \end{bmatrix} - \begin{bmatrix} \bar{y} \\ \bar{z} \\ 0 \\ 0 \\ \alpha_0 \\ \beta_0 \\ 0 \\ 0 \end{bmatrix} \quad (33)$$

The study determines the system matrix  $\mathbf{A}$  of the hose-drogue system using its physical properties. The matrix, represented by Eq.(34), describes the system in the absence of control surfaces. The effects of factors such as the frictional resistance of the ball joint  $b_f$  at the hose-drogue junction and the aerodynamic forces and moments due to the drogue's AOA and AOSS are modeled using Eqs. (35) and (36). The dynamic pressure of the atmospheric environment plays a crucial role in these equations and is denoted by the variable  $q$ .

$$\mathbf{A} = \begin{bmatrix} \mathbf{0}_{2 \times 2} & \mathbf{I}_{2 \times 2} & \mathbf{0}_{2 \times 2} & \mathbf{0}_{2 \times 2} \\ \mathbf{0}_{2 \times 2} & \mathbf{0}_{2 \times 2} & \mathbf{A}_{\text{Faero}} & \mathbf{0}_{2 \times 2} \\ \mathbf{0}_{2 \times 2} & \mathbf{0}_{2 \times 2} & \mathbf{0}_{2 \times 2} & \mathbf{I}_{2 \times 2} \\ \mathbf{0}_{2 \times 2} & \mathbf{0}_{2 \times 2} & \mathbf{A}_{\omega\text{aero}} & -b_f \mathbf{I}_{2 \times 2} \end{bmatrix} \quad (34)$$

$$\mathbf{A}_{\text{Faero}} = \frac{q}{m_{\text{drogue}}} \begin{bmatrix} 0 & 0 & 1 \\ 0 & 1 & 0 \end{bmatrix} \mathbf{L}_w^r \begin{bmatrix} C_{D\alpha} & C_{D\beta} \\ C_{Y\alpha} & C_{Y\beta} \\ C_{L\alpha} & C_{L\beta} \end{bmatrix} \quad (35)$$

$$\mathbf{A}_{\omega\text{aero}} = q \begin{bmatrix} 0 & 1 & 0 \\ 0 & 0 & 1 \end{bmatrix} (\mathbf{I}_{\text{drogue}}^R)^{-1} \mathbf{L}_w^r \begin{bmatrix} C_{mra} & C_{mr\beta} \\ C_{mpa} & C_{mp\beta} \\ C_{mya} & C_{my\beta} \end{bmatrix} \quad (36)$$

Eq.(35) expresses the relationship between important aerodynamic terms used in determining the forces experienced by a system. Eq.(36) is used to study the rotational aerodynamics of a drogue and involves the rotational inertia of the drogue described as  $\mathbf{I}_{\text{drogue}}^R$ . Specifically, it is used to estimate the AOA and AOSS by integrating the inertial angular velocity using this equation, which is used to determine the moments acting on the drogue. However, it should be noted that this approximation may not be completely precise.

The system utilizes Eq.(37) to define the control sensitivity matrix  $\mathbf{B}$  whereas Eq.(38) defines the linear actuation terms that relate to the forces generated by the actuators involved in controlling the position of the drogue. On the other hand, Eq.(39) defines the rotational control surfaces that are used to control the orientation of the drogue during flight.

$$\mathbf{B} = \begin{bmatrix} \mathbf{0}_{2 \times 4} \\ \mathbf{B}_F \\ \mathbf{0}_{2 \times 4} \\ \mathbf{B}_\omega \end{bmatrix} \quad (37)$$

$$\mathbf{B}_F = \frac{q}{m_{\text{drogue}}} \begin{bmatrix} 0 & 0 & -1 \\ 0 & -1 & 0 \end{bmatrix} \mathbf{L}_d^R \begin{bmatrix} C_{Du1} & C_{Du2} \\ C_{Yu1} & C_{Yu2} \\ C_{Lu1} & C_{Lu2} \end{bmatrix} \quad (38)$$

$$\mathbf{B}_\omega = q \begin{bmatrix} 0 & -1 & 0 \\ 0 & 0 & -1 \end{bmatrix} (\mathbf{I}_{\text{drogue}}^R)^{-1} \mathbf{L}_d^R \begin{bmatrix} C_{mru1} & C_{mru2} \\ C_{mpu1} & C_{mpu2} \\ C_{myu1} & C_{myu2} \end{bmatrix} \quad (39)$$

The values of the weighting matrices  $\mathbf{Q}$  and  $\mathbf{R}$  in the LQR controller are typically set through a process of trial and error. The selection of appropriate  $\mathbf{Q}$  and  $\mathbf{R}$  values is crucial, as they directly influence the behavior of the LQR controller and its ability to achieve desired control objectives while considering operational constraints. The matrix  $\mathbf{Q}$  represents the importance assigned to each state variable in the system's response. Higher values for elements in  $\mathbf{Q}$  imply a greater emphasis on minimizing the deviations. Adjusting the values in  $\mathbf{Q}$  prioritizes minimizing the deviations on certain states based on the control objectives.

The matrix  $\mathbf{R}$  represents the relative importance of control efforts or costs associated with dif-

ferent control inputs. Larger values for elements in  $R$  imply the preference for minimizing control effort. By adjusting the values in  $R$ , the controller's preference for control inputs can be adjusted, allowing for the limitation of excessive control effort or saturation.

After selecting appropriate weighting matrices  $Q$  and  $R$ , the Riccati equation is solved to obtain a unique positive semi-definite matrix solution  $P$  ( $P = P^T > 0$ ), which represents the optimal feedback gain. The Riccati equation is an algebraic equation of the form

$$A^T P + PA + Q - PBR^{-1}B^T P = 0 \quad (40)$$

The optimal input for the control surface is expressed as

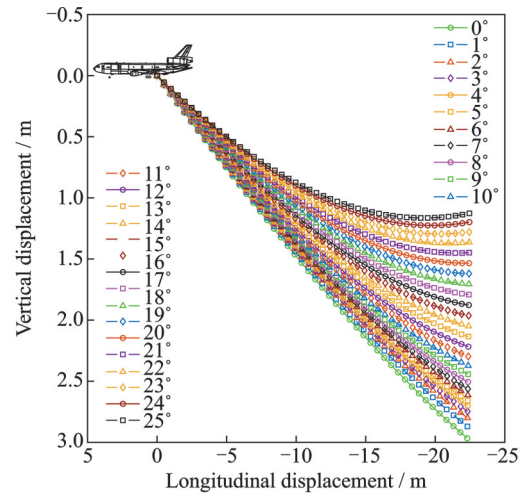
$$u = -R^{-1}B^T Px \quad (41)$$

The state vector  $x$ , the solution of Riccati equation  $P$ , the positive definite weighting matrix for control  $R$ , and the control sensitivity matrix  $B$  are used in the equation to obtain the optimal input to control the surface and stabilize the drogue at the desired position. This formula also enables the LQR controller's cost function to be minimized, ensuring optimal control and effective stabilization of the drogue.

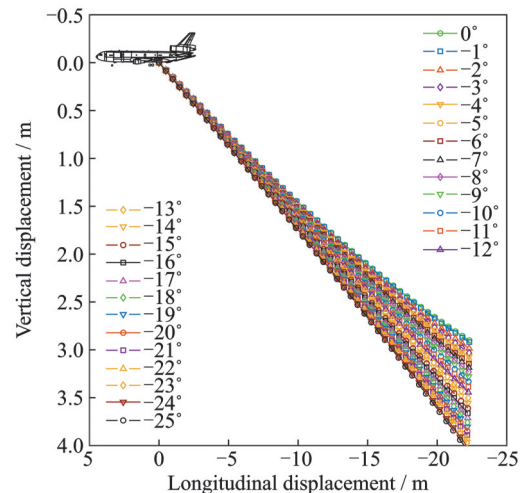
#### 4.2 Simulation and modeling of hose steady-state positioning and control

A static model is developed using multi-rigid body dynamics and force equilibrium principles to calculate the impact of control surfaces and other factors on the position of the hose. The primary focus of the study is on determining the steady-state hose position specifically under the influence of control forces generated by control surfaces. This model provides a simplified mathematical representation that can predict the potential impact of different factors on the position of the hose without the need for real-time simulations.

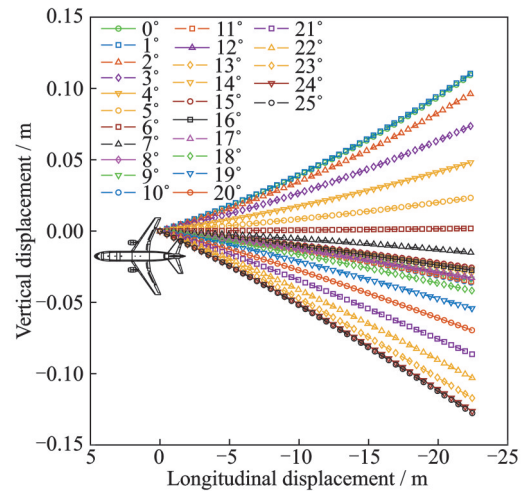
Fig.14 includes three sub-figures that depict the steady-state hose position in response to various control inputs. It shows the effect of the control force on the displacements of the hose-drogue assembly. Specifically, Fig.14(a) shows the steady-state hose position when the horizontal control surfaces are deflected downwards, while Fig.14(b) depicts the steady-state hose position when the horizontal con-



(a) Hose positioning with horizontal control surface deflected downwards



(b) Hose positioning with control surface deflected upwards



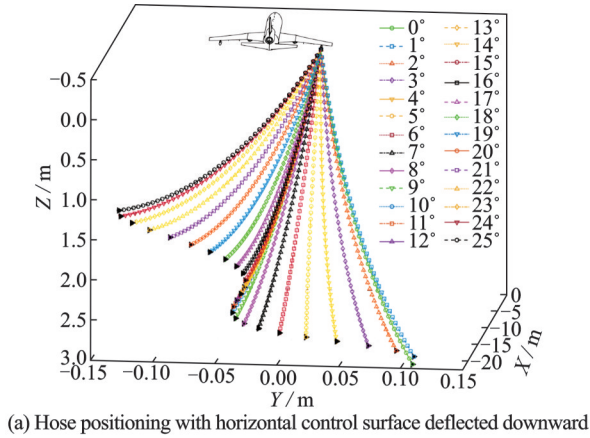
(c) Lateral displacement with horizontal control surface deflected downwards

Fig.14 Hose-drogue assembly displacements in response to horizontal control surface deflections

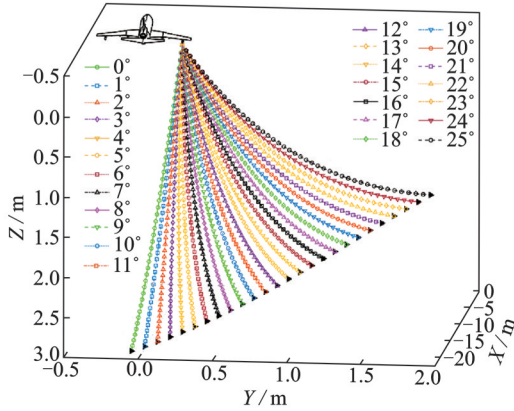
rol surfaces are deflected upwards. Fig.14(c) shows the displacement of the hose position when the horizontal control surfaces are deflected downwards. Additionally, note that the aircraft image shown in Fig.14 is not drawn to scale and is intend-

ed solely as a visual aid. However, these figures provide valuable insights into the behavior of the hose under different control conditions.

In addition, Fig.15(a) shows the steady-state position of the hose with the horizontal control surfaces input only. Fig.15(b) shows the steady-state position of the hose with both the horizontal and ver-

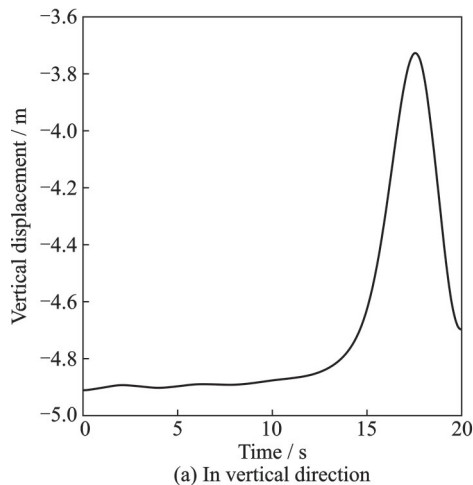


(a) Hose positioning with horizontal control surface deflected downward

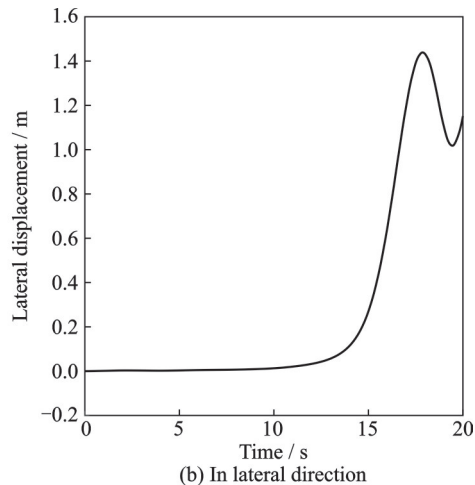


(b) Hose positioning with control surface deflected downwards and leftwards

Fig.15 Comparison between the results of deflecting horizontal control surfaces and both horizontal and vertical control surfaces



(a) In vertical direction



(b) In lateral direction

Fig.16 Displacements of the hose-drogue assembly in both vertical and lateral directions due to bow wave of receiver aircraft

tical control surfaces deflected downwards and left. Both figures provide additional insight into the control behavior of the hose system when both axes of control are utilized. The results also show that deflecting the horizontal control surface induces a yawing moment, with a displacement of up to 0.128 m at 25° of deflection.

### 4.3 Control effectiveness assessment during turbulence and bow wave simulations

This paper proposes a simulation and control system for mitigating the effects of bow waves and turbulence disturbance in the hose-drogue model. The simulation system is built using the Simscape/Multibody module in MATLAB/Simulink and incorporates modules such as a LQR controller, disturbances module, and an aerodynamic force model. The hose-drogue system, which is a critical component of the hose-drogue model, is simulated to assess its performance in reducing the disturbance caused by the bow wave and turbulence. The simulation process assumes perfect measurement of atmospheric conditions, drogue position and attitude, to obtain accurate results.

Fig.16 shows the displacement of the hose-drogue assembly in both the vertical and lateral directions during the bow wave disturbance. The bow wave effect significantly impacts the displacements of the hose-drogue assembly. As the refueling probe approaches the drogue, the airflow around the receiver's nose pushes the drogue away, causing an upward and outward motion, which explains the drastic change in the displacements.

Fig.17 shows the displacements of the hose-drogue assembly in both the vertical and lateral directions during the bow wave disturbance. Fig.18 depicts the displacement of the hose-drogue assembly in both the vertical and lateral directions under the influence of turbulence and bow waves with and without the control input. Without control, the drogue exhibits a motion of upward and outward oscillation in response to the disturbances. However, with control activated, the simulation results demonstrate an effective stabilization of the drogue position, with deviations from the reference point being

less than 10 cm throughout the entire docking process. This level of precision is well within the safety requirements and is indicative of the successful use of the control strategy for safe docking.

The simulation results demonstrate the effectiveness of the proposed control and mitigation system in significantly reducing the bow wave and turbulence disturbance. The simulations also reveal that the hose-drogue system can effectively reduce the disturbance caused by the bow wave and turbulence, thereby improving the performance of the hose-drogue model.

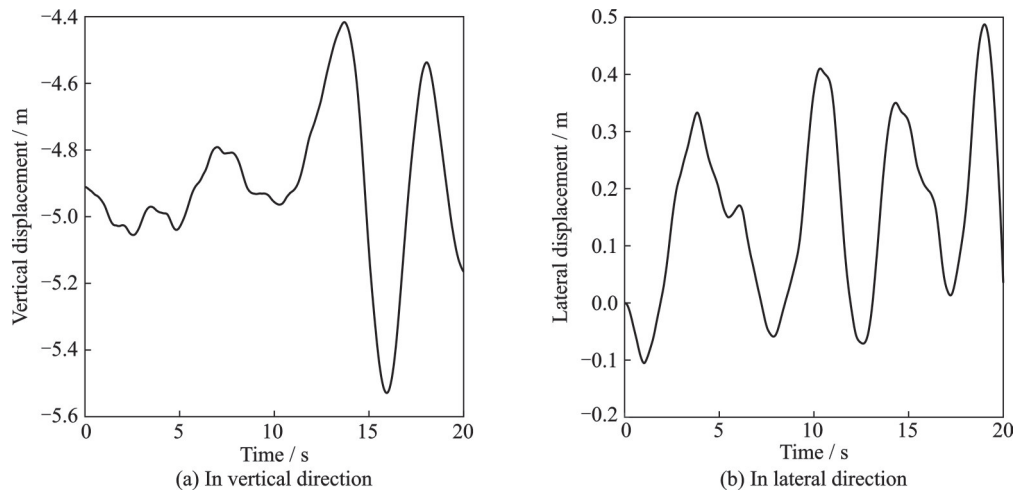


Fig.17 Displacements of the hose-drogue assembly in both vertical and lateral directions due to dryden wind turbulence

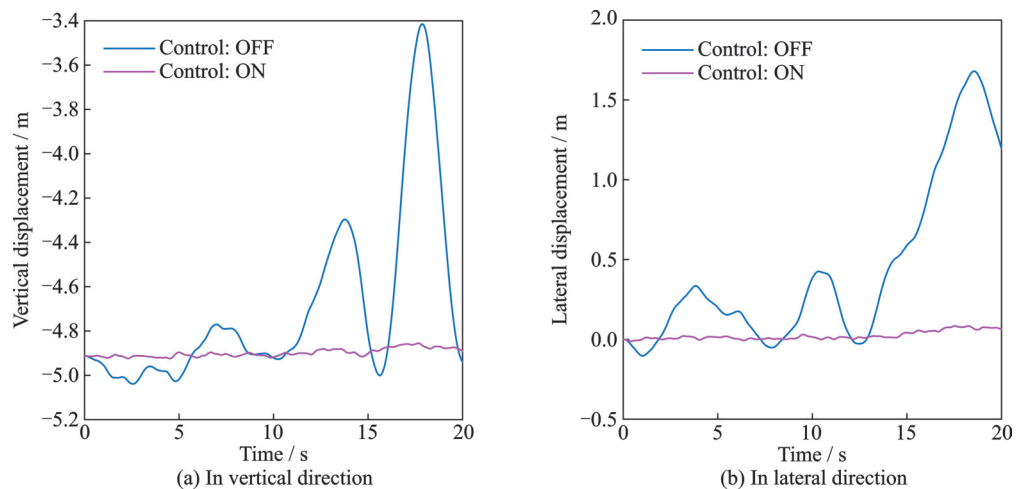


Fig.18 Displacements of the hose-drogue assembly when the control is turned ON and OFF

## 5 Conclusions

This article describes an actively stabilized drogue that has four control surfaces attached to it. By changing the deflection angles of the control surfaces, control force is generated to counteract distur-

bances caused by the bow wave effect and turbulence, resulting in a stabilized drogue. Numerical simulations are conducted to obtain the aerodynamic characteristics of the actively controlled stabilized drogue, which are then fitted using both linear and polynomial aerodynamics models. The drogue can

achieve controllability in motion when integrated with a control system.

Additionally, a simulation system is established based on the Simscape/Multibody module, which consists of a hose-drogue system, a LQR controller module, an aerodynamic module, and a combined disturbance module caused by the bow wave of the receiver aircraft and the wind turbulence. The effectiveness of the designed active controllable stabilizing drogue against combined disturbances, such as changes in velocity and force, is verified.

Numerical simulations are performed using a static program to determine the steady-state position of a hose corresponding to various deflection angles of the control surfaces. The objective of the simulations is to confirm the controllability of control surfaces in altering the position of the drogue in relation to aircraft.

Additionally, it is important to discuss the limitations or disadvantages of the proposed design, as well as mention any potential further developments and applications of this strategy. Here's how these aspects can be addressed concisely:

(1) Although the LQR controller offers several advantages such as simplicity and effectiveness in mitigating disturbances, it is essential to acknowledge its limitations. For example, the LQR controller assumes a linear and time-invariant system model, which may not accurately represent real-world dynamic systems with nonlinearities or time-varying characteristics. Additionally, the controller's performance heavily relies on the availability of accurate system dynamics and state feedback. One potential avenue for future work is to explore and implement alternative control strategies, such as nonlinear control and adaptive control, and to enhance the performance and robustness of the system beyond the limitations of the LQR controller.

(2) It is important to note that this study does not include a detailed parameterized study of the control surface nor a comprehensive examination of various initial conditions, particularly in terms of environmental factors. These aspects represent areas for further exploration. Future work will include a detailed parameterized study of the control surface to deepen our understanding of the influence of dif-

ferent design parameters on the system's response and performance. Additionally, this study will rigorously examine the multiplicity of initial conditions, particularly focusing on variations in environmental factors. This comprehensive approach aims to provide robust and versatile insight into the system's behavior in diverse scenarios, thereby enhancing the reliability and applicability of the research outcomes.

In conclusion, actively controllable stabilizing drogue technology has been developed to mitigate the challenges presented by the unstable random motion of the hose-drogue system during aerial refueling. This technology provides a stable target for pilots, improves aerial refueling accuracy, reduces risks, and enhances the overall effectiveness of aerial refueling operations. Additionally, the development of autonomous aerial refueling has become a major trend, necessitating a more intelligent aerial refueling process. Actively stabilized drogue technology can provide a solution for the safe docking of both manned and unmanned aircraft during the refueling process. A stable hose-drogue system is a critical aspect of this solution, improving the safety and accuracy of the docking process. Further research and development in this area can pave the way for more effective and efficient aerial refueling operations, making significant contributions to the aviation industry.

## References

- [1] BOLKCOM C. Air force aerial refueling methods: Flying boom versus hose-and-drogue[R]. [S.l.]: Congressional Research Service (CRS), 2006.
- [2] HANSEN J, MURRAY J, CAMPOS N. The NASA Dryden AAR project: A flight test approach to an aerial refueling system[C]//Proceedings of AIAA Atmospheric Flight Mechanics Conference and Exhibit. Providence, Rhode Island, USA: AIAA, 2004.
- [3] RO K, AHMAD H, KAMMAN J. Dynamic modeling and simulation of hose-paradrogue assembly for mid-air operations[C]//Proceedings of AIAA Infotech@Aerospace Conference. Seattle, Washington, USA: AIAA, 2009.
- [4] RO K, KAMMAN J W. Modeling and simulation of hose-paradrogue aerial refueling systems[J]. *Journal of Guidance, Control, and Dynamics*, 2010, 33(1): 53-63.
- [5] RO K, KUK T, KAMMAN J. Active control of aerial refueling hose-drogue systems[C]//Proceedings of AIAA Guidance, Navigation, and Control Confer-

- ence. Toronto, Ontario, Canada; AIAA, 2010.
- [6] RO K, KUK T, KAMMAN J. Design, test and evaluation of an actively stabilized drogue refueling system[C]//Proceedings of Infotech@Aerospace 2011. St. Louis, Missouri; AIAA, 2011.
- [7] BHANDARI U, THOMAS P R, RICHARDSON T S. Bow wave effect in probe and drogue aerial refueling[C]//Proceedings of AIAA Guidance, Navigation, and Control (GNC) Conference. Boston, MA: AIAA, 2013.
- [8] FELDMANN M S. Controllable drogue: US2010000 1124A1[P]. 2010-01-07.
- [9] WILLIAMSON W R, REED E, GLENN G J, et al. Controllable drogue for automated aerial refueling[J]. Journal of Aircraft, 2010, 47(2): 515-527.
- [10] ANON. Flying qualities of piloted aircraft department of defense handbook: MIL-HDBK—1997[R]. Washington, DC: U.S. Department of Defense, 1997.
- [11] ANON. Flying qualities of piloted airplanes: U.S. Military specification MIL-F-8785c[R]. Washington, DC: U.S. Department of Defense, 1980.
- [12] CHEN L. Research on aerodynamic compatibility and dynamic characteristics of hose drogue aerial refueling system[D]. Nanjing, China: Nanjing University of Aeronautics and Astronautics, 2016. (in Chinese)
- [13] LÖHNER R. Robust, vectorized search algorithms for interpolation on unstructured grids[J]. Journal of Computational Physics, 1995, 118(2): 380-387.
- [14] SPALART P, ALLMARAS S. A one-equation turbulence model for aerodynamic flows[C]//Proceedings of the 30th Aerospace Sciences Meeting and Exhibit. Reno, NV, USA: AIAA, 1992.
- [15] ARGYROPOULOS C D, MARKATOS N C. Recent advances on the numerical modelling of turbulent flows[J]. Applied Mathematical Modelling, 2015, 39(2): 693-732.
- [16] MAGHFIROH H, ATAKA A, WAHYUNG-GORO O, et al. Optimal energy control of DC motor speed control: Comparative study[C]//Proceedings of 2013 International Conference on Computer, Control, Informatics and Its Applications (IC3INA). Jakarta, Indonesia; IEEE, 2013: 89-93.
- [17] DHEWA O A, DHARMAWAN A, PRIYAMBO DO T K. Model of linear quadratic regulator (LQR) control method in hovering state of quadrotor[J]. Journal of Telecommunication, Electronic and Computer Engineering, 2017, 9(3): 135-143.

**Authors** Mr. NIO Zi Feng received his B.S. degree from South East Technological University, Ireland, and now he is pursuing the M.S. degree at Nanjing University of Aeronautics and Astronautics (NUAA). His research interests are in the aerodynamics field.

Prof. LIU Xueqiang received his B.S., M.S., and Ph.D. degrees from NUAA in 1997, 1999, and 2002, respectively. He served as a research assistant at Cranfield University in the United Kingdom from October 2001 to December 2002, at the University of Sheffield in the UK from June 2004 to October 2004, and at both the University of Sheffield and Rolls-Royce in the UK from January 2006 to June 2006. He has been a professor of NUAA since 2004. His research interests are in aerodynamics and aircraft design.

**Author contributions** Mr. NIO Zi Feng completed the modeling of the system, conducted the numerical simulations, interpreted the results, and wrote the manuscript. Mr. ZOU Guiyun participated in the modeling of the system. Prof. LIU Xueqiang provided guidance and support throughout the study by suggesting specific methodologies, reviewing the manuscript, and providing feedback. All authors commented on the manuscript draft and approved the submission.

**Competing interests** The authors declare no competing interests.

(Production Editor: WANG Jing)

## 考虑气动干扰下的可控锥套建模和软管锥套系统仿真

梁梓峰, 邹贵云, 刘学强

(南京航空航天大学航空学院, 南京 210016, 中国)

**摘要:** 开发了一个具有4个控制面的主动控制软管锥套的动态模型, 以减轻头波效应和紊流在对接阶段对空气动力干扰。使用数值模拟计算了软管锥套的空气动力特性, 并使用线性和多项式函数进行简化。利用空气动力模型设计了一个线性二次调节器(Linear quadratic regulator, LQR)控制器。使用MATLAB/Simulink构建了一个软管锥套模型, 并验证了主动控制软管锥套在减少干扰效应方面的效力。还使用静态模型研究了控制面偏转角对软管悬挂曲线的影响。数值模拟结果表明, 主动控制软管锥套降低了头波效应和紊流的干扰影响, 提高了软管锥套系统的稳定性和空中加油的成功率。

**关键词:** 主动增稳锥套; 软式空中加油; 计算流体力学; 气动干扰; LQR控制器